A&A 622, A180 (2019)
https://doi.org/10.1051/0004-6361/201732487

Astronomy & Astrophysics

J-PLUS: Measuring Hα emission line fluxes in the nearby universe

R. Logroño-García[1], G. Vilella-Rojo[1], C. López-Sanjuan[2], J. Varela[2], K. Viironen[2], D. J. Muniesa[1], A. J. Cenarro[2], D. Cristóbal-Hornillos[2], A. Ederoclite[2], A. Marín-Franch[2], M. Moles[2], H. Vázquez Ramió[1], S. Bonoli[2], L. A. Díaz-García[1], A. Orsi[1], I. San Roman[1], S. Akras[3], A. L. Chies-Santos[4], P. R. T. Coelho[5], S. Daflon[3], M. V. Costa-Duarte[5], R. Dupke[3,6], L. Galbany[7], R. M. González Delgado[8], J. A. Hernandez-Jimenez[5], R. Lopes de Oliveira[9,3,10,11], C. Mendes de Oliveira[5], I. Oteo[11,12], D. R. Gonçalves[13], M. Sánchez-Portal[14], L. Schmidtobreick[15], and L. Sodré Jr.[5]

(Affiliations can be found after the references)

Received 18 December 2017 / Accepted 8 June 2018

ABSTRACT

In this paper we aim to validate a methodology designed to obtain Hα emission line fluxes from J-PLUS photometric data. J-PLUS is a multi narrow-band filter survey carried out with the 2 deg^2 field of view T80Cam camera, mounted on the JAST/T80 telescope in the OAJ, Teruel, Spain. The information of the twelve J-PLUS bands, including the *J*0660 narrow-band filter located at rest-frame Hα, is used over the first 42 deg^2 observed to retrieve de-reddened and [NII] decontaminated Hα emission line fluxes of 46 star-forming regions with previous SDSS and/or CALIFA spectroscopic information. The agreement between the J-PLUS Hα fluxes and those obtained with spectroscopic data is remarkable, finding a median comparison ratio with a scatter of $\mathcal{R} = F_{\mathrm{H}\alpha}^{\mathrm{J-PLUS}}/F_{\mathrm{H}\alpha}^{\mathrm{spec}} = 1.05 \pm 0.25$. This demonstrates that it is possible to retrieve reliable Hα emission line fluxes from J-PLUS photometric data. With an expected area of thousands of square degrees upon completion, the J-PLUS dataset will allow the study of several star formation science cases in the nearby universe, as the spatially resolved star formation rate of nearby galaxies at $z \leq 0.015$, and how it is influenced by the environment, morphology, stellar mass, and nuclear activity. As an illustrative example, the close pair of interacting galaxies NGC 3994 and NGC 3995 is analysed, finding an enhancement of the star formation rate not only in the centre, but also in outer parts of the disk of NGC 3994.

Key words. methods: data analysis – techniques: photometric – galaxies: star formation

1. Introduction

The formation and evolution of galaxies is greatly influenced by the rate at which the available gas is converted into stars, namely, the star formation rate (SFR). Characterizing the SFR of galaxies at different epochs, and its relation with environment (e.g. Koyama et al. 2013), morphology (e.g. Willett et al. 2015), stellar mass (e.g. Speagle et al. 2014), or nuclear activity (e.g. Santini et al. 2012) among others, gives us a general picture of how galaxies form and evolve across cosmic time.

The physical processes occurring at the formation phase of stars yield observational hints in different wavelength ranges that can be used as tracers of star formation (Kennicutt & Evans 2012; Calzetti 2013). Stars are born in molecular gas clouds in which the newborn ones ionize the surrounding hydrogen with their ultraviolet emission. Following this, the recombination of hydrogen causes the emission of photons with wavelengths included in the hydrogen spectral series, such as those with Hα wavelength ($n = 3$ to $n = 2$ transition). The fact that Hα rest-frame wavelength lies in the optical range of the spectrum and is less affected by both dust and atmospheric extinction than other tracers, make it an easily detectable emission line, and hence a suitable tracer to study the SFR in the nearby universe (e.g. Kennicutt 1998; Catalán-Torrecilla et al. 2015).

Large spectroscopic and photometric surveys, such as the Sloan Digital Sky Survey (SDSS, York et al. 2000), have revolutionized astrophysics in many fields, but can only deliver a limited view of the star formation activity in the local universe, given that instruments have a small field of view (FoV) in the case of spectroscopic surveys, and a low spectral resolution in the case of photometric ones. In recent years, integral field spectroscopic (IFS) surveys such as the Calar Alto Legacy Integral Field spectroscopy Area (CALIFA, Sánchez et al. 2012a) survey used in this work, have overcome these problems with the use of instruments with larger FoVs and a fully spectral coverage (e.g SAURON, Bacon et al. 2001; ATLAS^{3D}, Cappellari et al. 2011; SAMI, Croom et al. 2012; VENGA, Blanc et al. 2013; and MaNGA, Bundy et al. 2015). However, these surveys still have limitations, such as the lack of a large contiguous observed area to trace the environment of nearby galaxies. They also suffer from selection biases due to the exclusion of galaxies with angular sizes that do not fit in the FoV of the integral field units (IFUs) that need to be considered (Walcher et al. 2014). These problems can be circumvented with multi-filter photometric surveys, which use a set of intermediate and narrow-band filters designed to provide the required spectral information while still covering a large contiguous area. The Javalambre Photometric Local Universe Survey (J-PLUS[1], Cenarro et al. 2019) is currently operating to observe thousands of square degrees of the northern sky from the Observatorio Astrofísico de Javalambre (OAJ[2]) in Teruel, Spain. The survey is being carried out with the 0.83 m JAST/T80 telescope and the panoramic camera T80Cam (Marin-Franch et al. 2015), with a 2 deg^2 FoV. A set of twelve broad, intermediate, and narrow-band optical filters is used (Fig. 1 and Table 1), optimized to provide an adequate sampling of the spectral energy distribution (SED) of millions of stars in our galaxy. These SEDs will be required for the photo-

[1] www.j-plus.es
[2] http://oajweb.cefca.es/

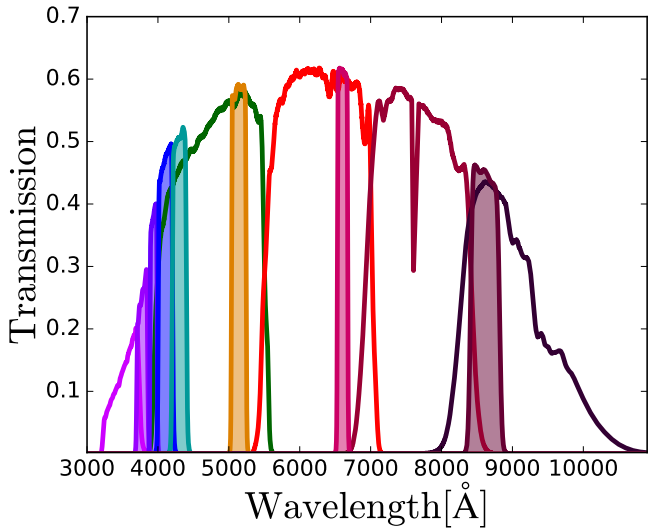

Fig. 1. Transmission curves of the J-PLUS filter system; with the four broad (g, r, i, z), the two medium $(u, J0861)$, and the six narrow $(J0378, J0395, J0410, J0430, J0515, J0660)$ band filters. The transmission curves were computed after accounting for the effects caused by the efficiency of the CCD and the atmospheric extinction.

metric calibration of the Javalambre Physics of the accelerating universe Astrophysical Survey (J-PAS[3], Benitez et al. 2014). In addition, the position of the filters, the exposure times, and the survey strategy, are suitable to perform science that will expand our knowledge in many fields of astrophysics. Further details on the OAJ, instrumentation, filter set, J-PLUS photometric calibration process, strategy, and several science applications can be found in the J-PLUS presentation paper (Cenarro et al. 2019).

Among all the possible science applications, our main interest is on star formation in the nearby universe ($z \leq 0.015$), where the Hα emission line flux is covered by the $J0660$ narrow-band filter. J-PLUS offers a large contiguous area mapped with twelve optical bands that enables us to: (1) have observations of the whole extent of galaxies, with no aperture selection effects; (2) carry out environmental studies; (3) count on a large statistical sample. These advantages are illustrated by showing the FoV of the T80Cam at JAST/T80 compared to the FoVs of several IFUs in Fig. 2. The main star formation science cases that can be addressed with the J-PLUS dataset are described below.

2D star formation properties. Benefiting from the characteristics of J-PLUS, it is possible to look into the spatially resolved star formation properties of nearby galaxies. With a large sample, the correlation of these properties with morphology (e.g. CALIFA: González Delgado et al. 2016), the presence of close companions (e.g. CALIFA: Barrera-Ballesteros et al. 2015; Cortijo-Ferrero et al. 2017), environmental density (e.g. SAMI: Schaefer et al. 2017), stellar mass (e.g. CALIFA: Cano-Díaz et al. 2016), or nuclear activity (e.g. MaNGA: Sánchez et al. 2018), among others, can be studied.

HII region statistical studies. It is possible to retrieve the excess of Hα flux over the underlying continuum in every pixel to construct HII region maps of spatially resolved galaxies. These maps allow the study of the properties of HII regions in individual galaxies (e.g. CALIFA: Sánchez et al. 2012b).

SFR density in the nearby universe. The Hα luminosity function in the nearby universe can be computed, and the SFR density at $z \leq 0.015$ calculated. Similar published studies are based on a selected sample of galaxies (e.g. Gallego et al. 1996; Pérez-González et al. 2003), but the depth and coverage of the J-PLUS observations allows the construction of a non-preselected catalogue of Hα emitters.

These topics will be presented in future publications, when the area surveyed by J-PLUS ensures a statistically meaningful sample of galaxies. Once J-PLUS has finalized its observations, it is expected to have data for approximately 5000 at $z \leq 0.015$. This represents a significant increase with respect to IFS surveys such as MaNGA, CALIFA, SAMI, or VENGA with 524, 251, 127, and 30 at the same redshift range, respectively (Wake et al. 2017; Sánchez et al. 2016a; Croom et al. 2012; Blanc et al. 2013).

To carry out the above science cases, a reliable measurement of the Hα flux from J-PLUS data is required. In a previous work, Vilella-Rojo et al. (2015) use synthetic photometry to predict that unbiased Hα fluxes can be retrieved from star-forming regions using the J-PLUS photometric system. The goal of the present paper is to test and validate the methodology presented by Vilella-Rojo et al. (2015) with real data, comparing the measured J-PLUS Hα emission line fluxes with spectroscopic ones from the literature. SDSS and CALIFA were chosen for this task so the comparison is performed with both spectroscopic fibre and integral field spectroscopic data, and because both datasets contain galaxies at $z \leq 0.015$. As of the date of this study, MaNGA currently released data did not contain any of the galaxies of the present work in this redshift range. The validation of the methodology would allow the study of the SFR in the neaby universe using the J-PLUS survey, and its southern counterpart, the Southern-Photometric Local Universe Survey (S-PLUS; Mendes de Oliveira & S-PLUS Collaboration, in prep.). S-PLUS will observe thousands of square degrees of the southern sky with an identical telescope, camera and filter-set than J-PLUS, making possible the use of all the tools and methodologies developed for the northern survey.

This paper is organized as follows. We present the J-PLUS and spectroscopic data used in this work in Sect. 2. Section 3 explains the processes of retrieving Hα emission line fluxes from the different datasets. In Sect. 4, the comparison between J-PLUS Hα fluxes and the spectroscopic ones is presented. The SFR science that will be tackled with J-PLUS is exposed with an example of the spatially resolved SFR in a close pair of galaxies in Sect. 5. Finally, we summarize the work done and present the conclusions in Sect. 6. A standard cosmology $H_0 = 70\,\mathrm{km\,s^{-1}\,Mpc^{-1}}$, $\Omega_\mathrm{m} = 0.3$, $\Omega_\Lambda = 0.7$ and $\Omega_\mathrm{k} = 0$ is used. Magnitudes are expressed in the AB system (Oke & Gunn 1983).

2. J-PLUS and spectroscopic data

In this section, the different datasets used in the present work are introduced. We first describe the processes of acquisition and reduction of J-PLUS photometric data, and give their main characteristics (Sect. 2.1). Then, the spectroscopic data from SDSS (Sect. 2.2) and the CALIFA survey (Sect. 2.3) utilized in this comparison study are commented.

2.1. J-PLUS photometric data

The photometric data used in this work were acquired with the 0.83 m JAST/T80 telescope and the panoramic camera T80Cam, set up with a 9216×9232 pixel CCD. The system offers a

[3] www.j-pas.org

Table 1. J-PLUS filters characteristics and limiting magnitudes.

Filter	Central wavelength (nm)	Pivot wavelength (nm)	*FWHM* (nm)	$m_{\rm lim}{}^a$ (SVD 1500041)	$m_{\rm lim}{}^a$ (EDR)	σ_{ZP}	Spectral feature
u	348.5	352.3	50.8	22.5	21.5	0.05	–
*J*0378	378.5	378.6	16.8	21.9	21.4	0.06	[OII]
*J*0395	395.0	395.1	10.0	21.3	21.3	0.07	CaH+K
*J*0410	410.0	410.1	20.0	21.0	21.4	0.06	H_δ
*J*0430	430.0	430.0	20.0	21.3	21.4	0.06	*G*-Band
g	480.3	474.5	140.9	23.1	22.1	0.05	–
*J*0515	515.0	515.0	20.0	21.4	21.3	0.04	Mg*b* Triplet
r	625.4	623.0	138.8	23.1	21.8	0.04	–
*J*0660	660.0	660.0	13.8	22.5	21.1	0.04	Hα+[NII]
i	766.8	767.7	153.5	22.0	20.7	0.04	–
*J*0861	861.0	860.3	40.0	22.1	20.6	0.05	Ca Triplet
z	911.4	892.2	140.9	21.2	20.5	0.02	–

Notes. [(a)] The limiting magnitudes were measured at a fixed 3″ aperture for a signal to noise ratio (S/N) of 3.

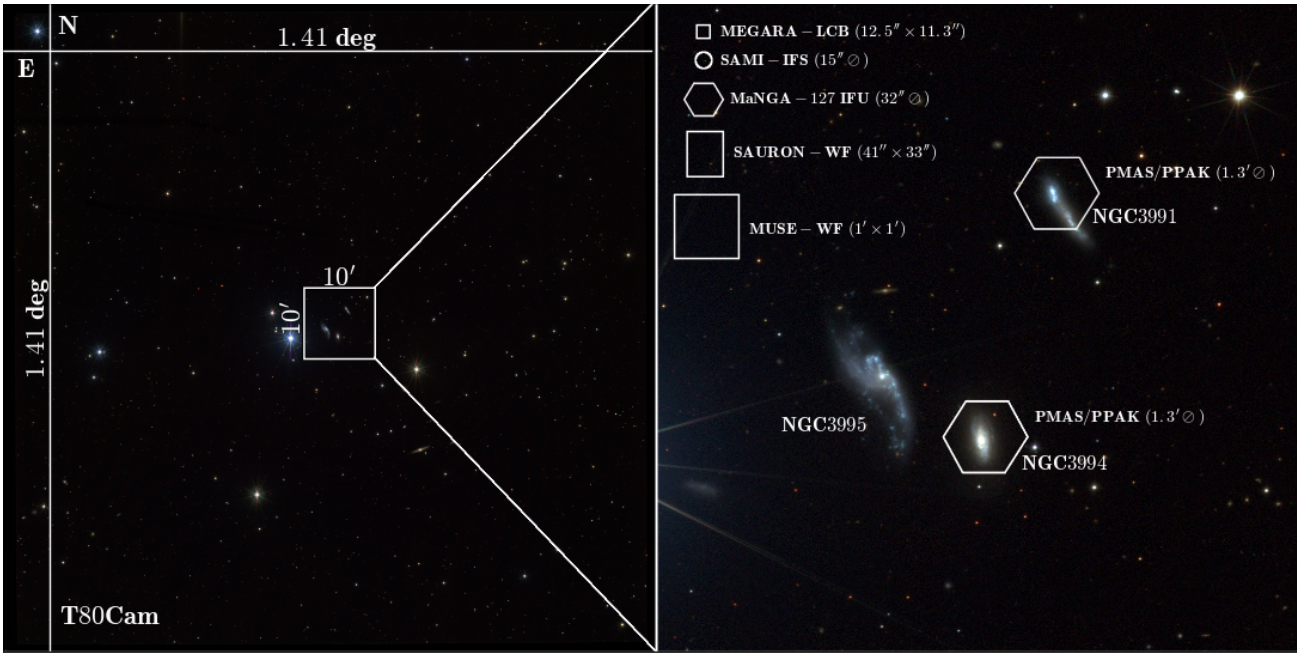

Fig. 2. *Left panel*: colour composite image of the SVD 1500041 pointing "1500041-Arp313", illustrating the 2 deg^2 FoV of T80Cam at JAST/T80. *Right panel*: 10′ × 10′ zoom on the Arp313 triplet, where the galaxies NGC 3991, NGC 3994, and NGC 3995 are higlighted. The FoV of several IFUs is displayed: MEGARA (Gil de Paz et al. 2016), SAMI (Croom et al. 2012), MaNGA (Bundy et al. 2015; Drory et al. 2015), SAURON (Bacon et al. 2001), MUSE (Bacon et al. 2010) and PMAS/PPAK (Roth et al. 2005; Sánchez et al. 2012a). NGC 3991 and NGC 3994 are part of the CALIFA DR3 sample (Sánchez et al. 2016a).

1.4×1.4 deg^2 FoV with a 0.55″/pixel scale. Figure 1 shows the transmission curves of the complete set of filters, and Table 1 displays their characteristics. The fields for the study were chosen to maximize the photometric measurements of star-forming regions in common with SDSS, and galaxies with star formation activity in common with CALIFA, both at $z \leq 0.015$. The final eight pointings selected belong to two different datasets. One is the J-PLUS Early Data Release (EDR), a subset of 36 deg^2 representative of J-PLUS data in terms of depth, point spread function (PSF), and photometric calibration accuracy (Cenarro et al. 2019). The other is a J-PLUS Science Verification Data project (SVD 1500041; PI: G. Vilella-Rojo), which was especially designed for the present work. The observations of the J-PLUS SVD 1500041 took place during several nights in February 2016 and on average, they are 0.85 mag deeper than J-PLUS EDR. These depths were required given that the project was planned to be part of the science verification phase of the T80Cam at JAST/T80 system. In the following, we refer to the joint SVD 1500041 and EDR data as "J-PLUS" data. Further details on the limiting magnitudes of both datasets and the characteristics of the selected fields can be found in Tables 1 and 2, respectively. In addition to the present research, the J-PLUS EDR and SVD were used to: refine the membership in nearby galaxy clusters (Molino et al. 2019), analyse the globular cluster M 15 (Bonatto et al. 2019), study the stellar populations of several local galaxies (San Roman et al. 2019), and compute the stellar and galaxy number counts up to $r = 21$ (López-Sanjuan et al. 2019).

Table 2. Description of the T80Cam pointings.

J-PLUS pointing	Central RA (°)	Central Dec (°)	SDSS star forming regions	CALIFA star forming galaxies	Comments
1500041-M101	211.105	54.650	8	–	M101 is present
1500041-Arp313	179.423	32.298	10	NGC 3991 & NGC 3994	Arp 313 triplet is present
1500041-M49	188.042	8.134	3	NGC 4470	M49 is present
JPLUS-00745	121.809	30.443	1	–	–
JPLUS-00749	128.213	30.443	1	–	–
JPLUS-01500	131.116	40.190	1	–	–
JPLUS-01506	141.923	40.190	1	–	–
JPLUS-01588	109.596	41.582	1	–	–

Once the observations were fulfiled; data reduction, photometric calibration, and image co-adding were automatically performed by different pipelines that are part of the `Jype` package, fully developed by the Data Processing and Archiving Unit (UPAD) team at CEFCA. The final products for every pointing include co-added images and weight maps in the twelve bands with calibration zero-points (*ZPs*), as well as photometric catalogues of the sources found. The uncertainties in the calibration (σ_{ZP}) can be seen in Table 1. Further details about the processes involved in the production of the images and catalogues are explained in Cenarro et al. (2019). In this study the co-added images were used, but before working with them, a PSF homogenization in the twelve-band images of each pointing was performed.

The homogenization of the PSF is required to provide good quality photometry, because the co-added images are constructed with different individual ones. This means that several exposures are combined to create a single final image, each of them not necessarily having the same PSF, which generates inhomogeneities in the light distribution of the sources in a given band. Additionally, the PSF associated with a certain object changes from one band to another. This turns into differences in the light distribution of the same object in a given aperture depending on the band where it is looked.

These effects on the PSF may produce artificial structures that could bias the results (Bertin 2011). To deal with them, we used the `JypePSF` module included in the `Jype` package. The `JypePSF` module analyses, characterizes, and homogenizes the PSF. The worst PSF value of each pointing was computed by checking the full width at half maximum of the PSF ($\mathrm{PSF_{FWHM}}$) of bright point sources in every band image. Then, the obtained value was selected as the target for the homogenization in the twelve bands; although the code also allows the user to choose the reference value. A homogenization kernel was created for different positions in every band image. In this step, `SExtractor` (Bertin & Arnouts 1996) and `PSFex` (Bertin 2013) were used. The band images were convolved with their corresponding kernels using a fast Fourier transform, bringing them to the same circular PSF. This process has consequences in background noise of the images. Therefore, the background noise model of the images was recalculated, since it was later used to compute photometric errors (Sect. 3.3). The correct performance of the PSF homogenization process could be checked by looking at the light profile of bright sources (Stefanon et al. 2017), as in the example in Fig. 3.

Two sets of J-PLUS images were prepared for every pointing, each one with a different median $\mathrm{PSF_{FWHM}}$, corresponding to the values of SDSS-DR12 and CALIFA-DR2. The median $\mathrm{PSF_{FWHM}}$ of the SDSS-DR12 images and spectra used in this work are 1.30″ (Alam et al. 2015) and 1.42″, respectively. These are similar to the one of the J-PLUS sample, 1.30″. Therefore, it is not necessary to re-homogenize the J-PLUS images to compare them with the SDSS data of the present work. In the case of CALIFA-DR2, the median $\mathrm{PSF_{FWHM}}$ is 2.4″ (García-Benito et al. 2015), due to the different spatial sampling, rather than to observing conditions (Fig. 4). A subsequent PSF homogenization of the J-PLUS images was performed, choosing the quoted target value, and yielding a more fair comparison.

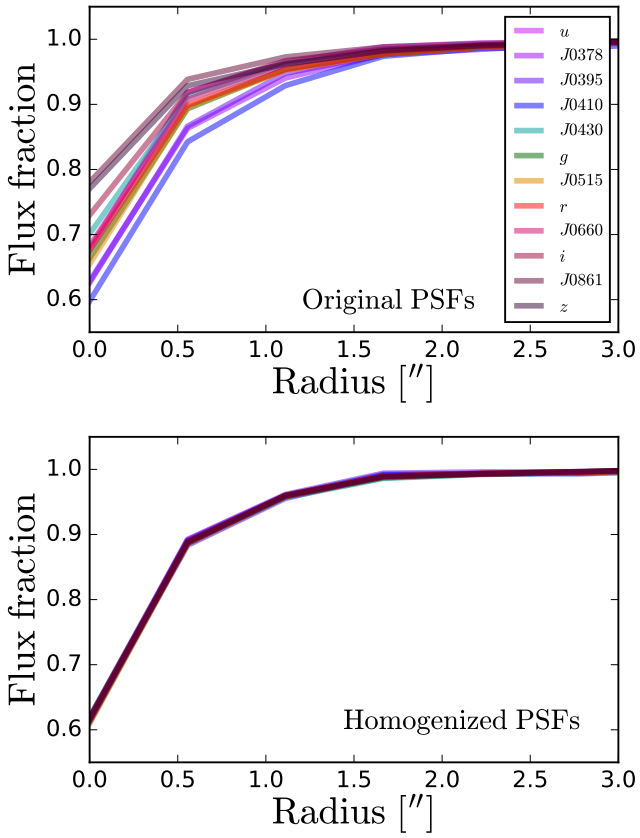

Fig. 3. Effect of the PSF homogenization on the light profile of a source. *Top*: lines with different colours correspond to the light profile of the source in the twelve *J-PLUS* bands. *Bottom*: light is equally distributed in every band after the homogenization, and the profiles are indistinguishible.

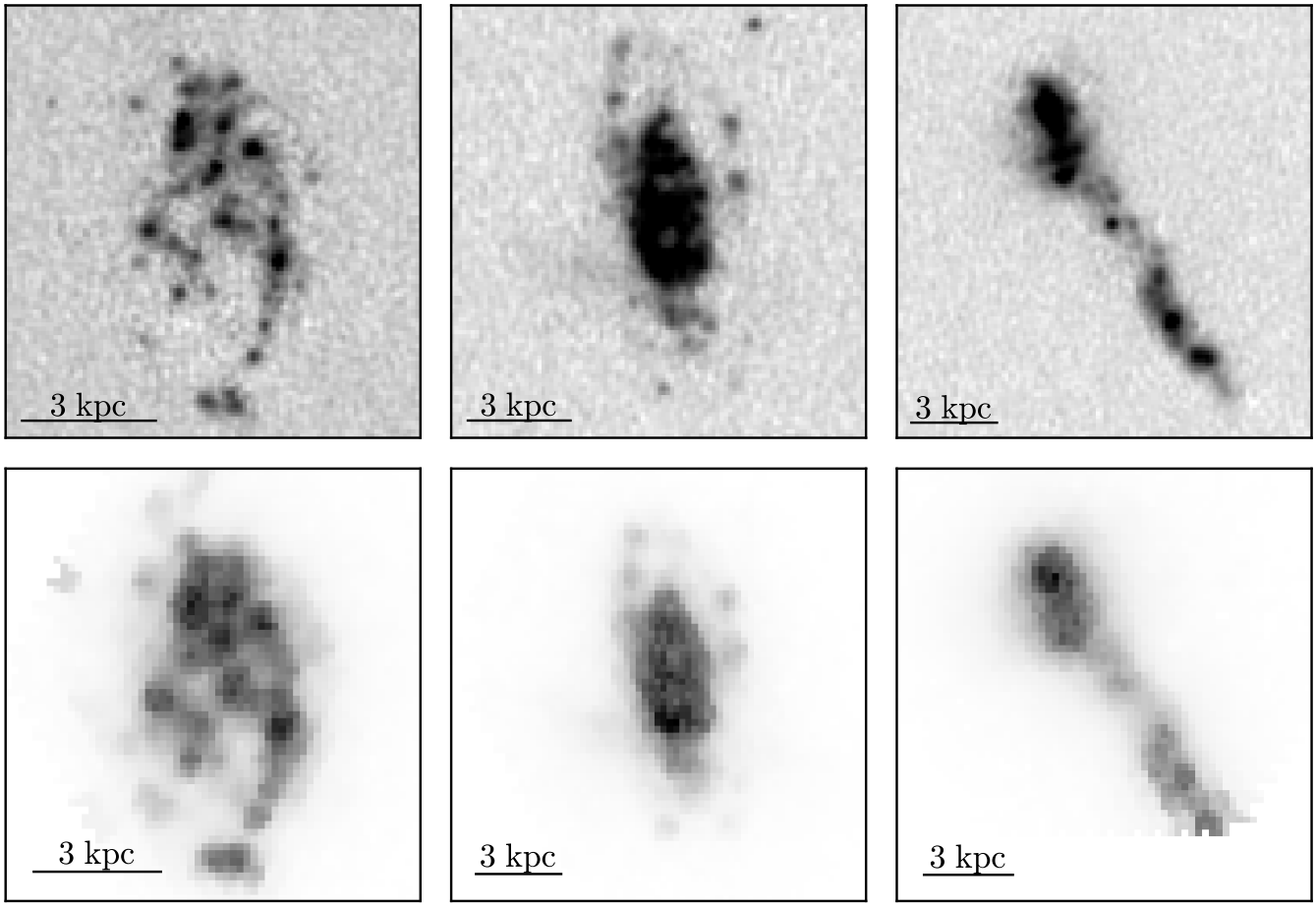

Fig. 4. J-PLUS images showing Hα emission areas with the flux excess in the J0660 band, $J0660-r$ (*top panels*), and CALIFA Hα maps (*bottom panels*) of the selected star-forming galaxies: NGC 4470 (*left panels*), NGC3994 (*centre panels*), and NGC 3991 (*right panels*). For reference, north is up and east is left.

2.2. SDSS data

The SDSS data used in this work, are emission line fluxes of star-forming regions measured by the Portsmouth group (Thomas et al. 2013) and their corresponding original spectra. They are part of the SDSS Data Release 12 (DR12, Alam et al. 2015; including BOSS). These fluxes were obtained from multiple fibre spectra observations of nearby galaxies, resulting from a wrong deblending due to the apparent large size of these objects (York et al. 2000; Strauss et al. 2002). They were collected with the Sloan foundation 2.5 m telescope at Apache Point observatory. The complete set of data is available for download in the DR12 website[4,5]. The emission line fluxes by Thomas et al. (2013) were estimated with an adaptation of the publicly available code Gas and Absorption Line Fitting code (`GANDALF v1.5`, Sarzi et al. 2006), by fitting stellar population models and Gaussian emission line templates to the spectra. The stellar population models from Maraston & Strömbäck (2011), based on the MILES stellar library, were used in this task.

2.3. CALIFA data

The CALIFA data used in the present work belong to the Data Release 2. They are based on observations collected at the Centro Astronómico Hispano Alemán (CAHA) at Calar Alto with the PMAS/PPAK integral field spectrophotometre, mounted on the Calar Alto 3.5 m telescope (Sánchez et al. 2012a; Walcher et al. 2014; García-Benito et al. 2015). Data products can be found in the CALIFA website[6], from which we downloaded the V500 data cubes of the galaxies included in the present study. The three CALIFA galaxies selected are star-forming spirals at $z \leq 0.015$ (Table 2).

In addition to the data cubes, Hα emission line fluxes of CALIFA galaxies are required to perform the comparison. We used the available data products provided by `Pipe3D` in the CALIFA-DR2 website[7], where Hα flux maps of the galaxies of this work are available (Fig. 4).

`Pipe3D` is a pipeline based on the `FIT3D` fitting tool (Sánchez et al. 2006, 2011). It was designed to study the properties of the stellar populations and ionized gas of IFS data, thus being a higlhy suitable tool for the analysis of the data cubes from ongoing and upcoming IFS surveys. Among the several steps performed by the pipeline, we highlight: (1) the stellar continuum fitting with stellar population models by the MILES project (Sánchez-Blázquez et al. 2006; Vazdekis et al. 2010; Falcón-Barroso et al. 2011). This is done on binned spaxels of the data cubes, according to S/N criteria; (2) the decoupling of every spaxel in the bins along with their own spectrum;

[4] https://dr12.sdss.org/advancedSearch
[5] http://www.sdss.org/dr12/spectro/galaxy_portsmouth
[6] www.caha.es/CALIFA/
[7] ftp://ftp.caha.es/CALIFA/dataproducts/DR2/Pipe3D/

Table 3. Positions and Hα emission line fluxes of the selected star-forming regions for the comparison between J-PLUS and the spectroscopic surveys.

Region	RA (º)	Dec (º)	$\log F^{\mathrm{J-PLUS}}_{\mathrm{H}\alpha}$ (10^{-17} erg s^{-1} cm^{-2})	$\log F^{\mathrm{spec}}_{\mathrm{H}\alpha}$ (10^{-17} erg s^{-1} cm^{-2})
CALIFA-NGC 4470-1	187.409	7.826	3.41 ± 0.07	3.39 ± 0.04
CALIFA-NGC 4470-2	187.407	7.827	3.28 ± 0.07	3.34 ± 0.02
CALIFA-NGC 4470-3	187.406	7.826	3.37 ± 0.07	3.35 ± 0.03
CALIFA-NGC 4470-4	187.408	7.825	3.34 ± 0.08	3.44 ± 0.04
CALIFA-NGC 4470-5	187.407	7.823	3.20 ± 0.09	3.25 ± 0.03
CALIFA-NGC 4470-6	187.410	7.823	3.27 ± 0.08	3.16 ± 0.04
CALIFA-NGC 4470-7	187.405	7.823	3.15 ± 0.08	3.22 ± 0.03
CALIFA-NGC 4470-8	187.405	7.822	3.37 ± 0.07	3.50 ± 0.03
CALIFA-NGC 3994-1	179.405	32.283	2.81 ± 0.07	2.77 ± 0.01
CALIFA-NGC 3994-2	179.400	32.280	2.90 ± 0.07	2.78 ± 0.01
CALIFA-NGC 3994-3	179.406	32.281	2.92 ± 0.07	2.90 ± 0.01
CALIFA-NGC 3994-4	179.404	32.271	2.21 ± 0.09	2.24 ± 0.01
CALIFA-NGC 3994-5	179.400	32.278	2.85 ± 0.07	2.64 ± 0.01
CALIFA-NGC 3994-6	179.402	32.273	2.80 ± 0.08	2.74 ± 0.01
CALIFA-NGC 3994-7	179.403	32.276	3.86 ± 0.07	4.35 ± 0.06
CALIFA-NGC 3994-8	179.403	32.277	4.09 ± 0.11	3.88 ± 0.04
CALIFA-NGC 3991-1	179.375	32.333	3.44 ± 0.07	3.78 ± 0.04
CALIFA-NGC 3991-2	179.381	32.339	3.52 ± 0.07	3.87 ± 0.03
CALIFA-NGC 3991-3	179.381	32.339	3.50 ± 0.07	3.73 ± 0.02
CALIFA-NGC 3991-4	179.382	32.341	3.94 ± 0.07	4.20 ± 0.04
SDSS-1627-53473-0554	188.194	7.799	2.07 ± 0.12	2.09 ± 0.02
SDSS-1627-53473-0611	188.576	8.239	3.64 ± 0.07	3.61 ± 0.02
SDSS-1628-53474-0323	188.589	8.240	3.16 ± 0.07	3.11 ± 0.04
SDSS-1323-52797-0108	209.971	54.786	3.11 ± 0.07	3.11 ± 0.01
SDSS-1324-53088-0183	211.388	54.461	3.74 ± 0.07	3.58 ± 0.01
SDSS-1324-53088-0386	210.135	55.246	2.79 ± 0.09	2.87 ± 0.01
SDSS-1325-52762-0398	211.341	54.269	2.96 ± 0.10	2.78 ± 0.04
BOSS-6739-56393-0662	210.827	54.589	1.84 ± 0.11	1.91 ± 0.01
BOSS-6797-56426-0464	211.384	54.459	2.13 ± 0.11	2.10 ± 0.01
BOSS-6797-56426-0488	210.919	54.496	1.80 ± 0.15	1.33 ± 0.04
BOSS-6801-56487-0008	212.111	54.908	2.35 ± 0.10	2.38 ± 0.03
SDSS-1991-53446-0553	178.927	32.188	3.32 ± 0.11	3.06 ± 0.05
SDSS-1991-53446-0571	179.168	32.628	2.56 ± 0.13	2.46 ± 0.01
SDSS-1991-53446-0587	179.435	32.298	3.53 ± 0.08	3.48 ± 0.02
SDSS-1991-53446-0588	179.427	32.284	3.42 ± 0.07	3.43 ± 0.01
SDSS-1991-53446-0592	179.135	32.130	2.33 ± 0.11	2.22 ± 0.01
SDSS-1991-53446-0600	179.096	32.038	2.54 ± 0.15	2.36 ± 0.04
SDSS-2095-53474-0311	179.142	32.128	2.38 ± 0.10	2.35 ± 0.01
SDSS-2095-53474-0352	179.381	32.339	3.79 ± 0.07	3.81 ± 0.02
SDSS-2095-53474-0355	179.433	32.294	4.02 ± 0.07	4.07 ± 0.03
BOSS-4601-55589-0198	179.427	32.285	2.70 ± 0.08	2.62 ± 0.02
SDSS-0860-52319-0468	121.067	30.182	2.92 ± 0.08	2.83 ± 0.04
SDSS-1208-52672-0399	127.416	31.077	3.44 ± 0.07	3.57 ± 0.01
SDSS-0829-52296-0434	130.908	40.429	2.67 ± 0.09	2.60 ± 0.01
SDSS-0939-52636-0081	142.065	40.149	2.75 ± 0.09	2.66 ± 0.01
SDSS-1864-53313-0249	110.280	41.127	2.77 ± 0.08	2.78 ± 0.01

(3) the fitting of the strongest spectral emission lines of every spaxel, and production of spatially resolved maps of the flux of these lines. Detailed information about `Pipe3D` can be found in Sánchez et al. (2016b,c).

3. Measuring Hα in the nearby universe

In this section, the steps to obtain the Hα emission line fluxes from spectroscopic data (Sects. 3.1 and 3.2), and from J-PLUS photometric data (Sect. 3.3) are explained. Our final goal is to obtain the emission line fluxes from the different datasets measured in the same regions, making the comparison presented in Sect. 4 possible.

3.1. Hα flux measurements from SDSS

As a first step to define the sample of star-forming regions with SDSS Hα flux estimates by the Portsmouth group, we initially selected all the sources with emission line measurements that lie

inside the J-PLUS fields used in the present work. Then, a series of selection criteria were applied to compose the final sample.

Firstly, only star-forming regions that are at $z \leq 0.015$ remained in the sample, since these are representative of those we deal with in J-PLUS. The Portsmouth group includes a classification according to a Baldwin, Phillips & Terlevich (BPT) diagram (Baldwin et al. 1981) for every source; we used this classification to choose sources that are classified as "Star Forming / HII", avoiding AGN contamination in the sample. This step is necessary since SDSS fibres are usually placed in the centre of galaxies, where AGN effects are expected to be more important.

Secondly, considering the equivalent width measurements of the lines by the Portsmouth group, we imposed a lower limit of 12 Å in the Hα equivalent width ($EW_{\mathrm{H}\alpha} \geq 12$ Å). This is done because J-PLUS instruments cannot resolve spectroscopically the Hα emission line with a 3σ precision if it has an equivalent width below that value (Eq. (13) in Vilella-Rojo et al. 2015).

The final sample contains 26 star-forming regions. The Hα fluxes and errors of the regions provided by the Portsmouth group are dust-corrected with Calzetti et al. (2000) dust extinction law. Numerical values are reported in Table 3.

3.2. Hα flux measurements from CALIFA

The `Pipe3D` Hα flux maps from CALIFA data (Sánchez et al. 2016b,c) were used to visually select star-forming region candidates. We placed 3″ diametre circular apertures, mimicking SDSS fibres, on the knots of star formation. Then we imposed them to fulfil the same criteria required for SDSS star-forming regions (Sect. 3.1). The pre-selected candidates are all at $z \leq 0.015$ with $EW_{\mathrm{H}\alpha} \geq 12$ Å. To obtain their BPT diagram, the fluxes from the different emission lines were retrieved with the `Pipe3D` flux maps available. The aperture measurements on the regions were carried out with the `funcnts` module included in the `funtools` package (Mandel et al. 2001). Once the emission lines were retrieved, the regions were placed in the BPT diagram (Fig. 5). The diagram is divided into HII, composite, and AGN zones (Kewley et al. 2001; Kauffmann et al. 2003). The 20 candidate star-forming regions are within the HII area, accomplishing the established criteria. Eight regions are included in both NGC 3994 and NGC 4470, and four are included in NGC 3991 (Table 3 and Fig. 6).

The Hα emission line fluxes of the CALIFA selected star-forming regions need to be corrected for dust extinction. To do so, we repeated the procedure applied to the SDSS data by using the Calzetti et al. (2000) extinction law with the Balmer decrement. The following expressions were computed:

$$F_{\mathrm{i}} = F_{\mathrm{o}} 10^{0.4E(B-V)k'(\lambda)} = F_{\mathrm{o}} 10^{1.33E(B-V)}, \tag{1}$$

where F_{i} and F_{o} represent the intrinsic and observed flux respectively, and $k'(\lambda) = 3.33$ for Hα. The colour excess $E(B-V)$ is

$$E(B-V) = 1.97 \log_{10}\left[\frac{(\mathrm{H}\alpha/\mathrm{H}\beta)_{\mathrm{o}}}{2.86}\right]. \tag{2}$$

The observed fluxes and errors of the regions were retrieved from `Pipe3D` flux maps with `funcnts`. The errors of the fluxes in a given aperture need to be calculated following the prescriptions in García-Benito et al. (2015). Numerical values of the Hα emission line fluxes of the CALIFA star-forming regions are reported in Table 3.

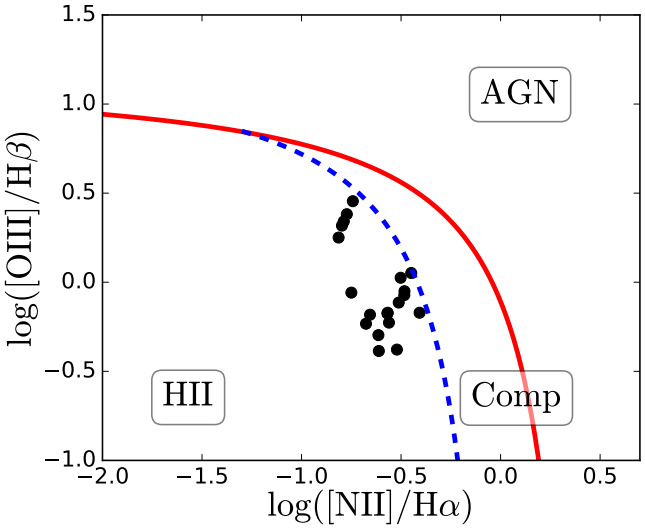

Fig. 5. BPT diagram based on CALIFA data of the 20 selected star-forming regions in NGC 3991, NGC 3994 and NGC 4470. The blue-dashed and red lines delimit the composite and AGN zone, respectively (Kewley et al. 2001; Kauffmann et al. 2003).

3.3. Flux meauserements from J-PLUS data

We retrieved a J-PLUS instrumental photometry catalogue of the SDSS and CALIFA star-forming regions, as a first step to estimate the J-PLUS Hα emission line fluxes of them. This was done performing aperture photometry on the twelve band images, mimicking the same spectroscopic locations (Table 3) and apertures, with the `funcnts` software. The instrumental photometry is measured in counts (C), expressed in analogue to digital units (ADUs), bringing up the requirement of converting it into flux. The flux density of a source in a given band is

$$F_\lambda = (C - C_{\mathrm{B}})\, 10^{-0.4(ZP+48.6)} \frac{c}{\lambda^2_{\mathrm{pivot}}}, \tag{3}$$

where C_{B} represents the background counts, ZP is the calibration zero point of the band, c is the speed of light, and λ_{pivot} is the pivot wavelength of the filter, which is a source-independent measurement of the characteristic wavelength of a bandpass given by

$$\lambda^2_{\mathrm{pivot}} = \frac{\int T(\lambda)\mathrm{d}\lambda}{\int \frac{T(\lambda)}{\lambda^2}\mathrm{d}\lambda}, \tag{4}$$

where $T(\lambda)$ represents the transmission curve of the filter. The λ_{pivot} values of the J-PLUS filters are shown in Table 1. To calculate the errors, it was necessary to account for three sources of uncertainty that affect the measurements: the uncertainty in the zero point (σ_{ZP}), the large-scale background noise variation ($\sigma_{C_{\mathrm{B}}}$), and the electron counting by the CCD (σ_C). The total uncertainty in the flux of a source in a certain band, is then given by

$$\sigma_{\mathrm{F}} = \sqrt{\left(\frac{\partial F_\lambda}{\partial ZP}\sigma_{ZP}\right)^2 + \left(\frac{\partial F_\lambda}{\partial C_{\mathrm{B}}}\sigma_{C_{\mathrm{B}}}\right)^2 + \left(\frac{\partial F_\lambda}{\partial C}\sigma_C\right)^2}, \tag{5}$$

where

$$\sigma_{C_{\mathrm{B}}} = S_{\mathrm{fit}} \sqrt{N_{\mathrm{pix}}}(a_{\mathrm{fit}} + b_{\mathrm{fit}} \sqrt{N_{\mathrm{pix}}}) \tag{6}$$

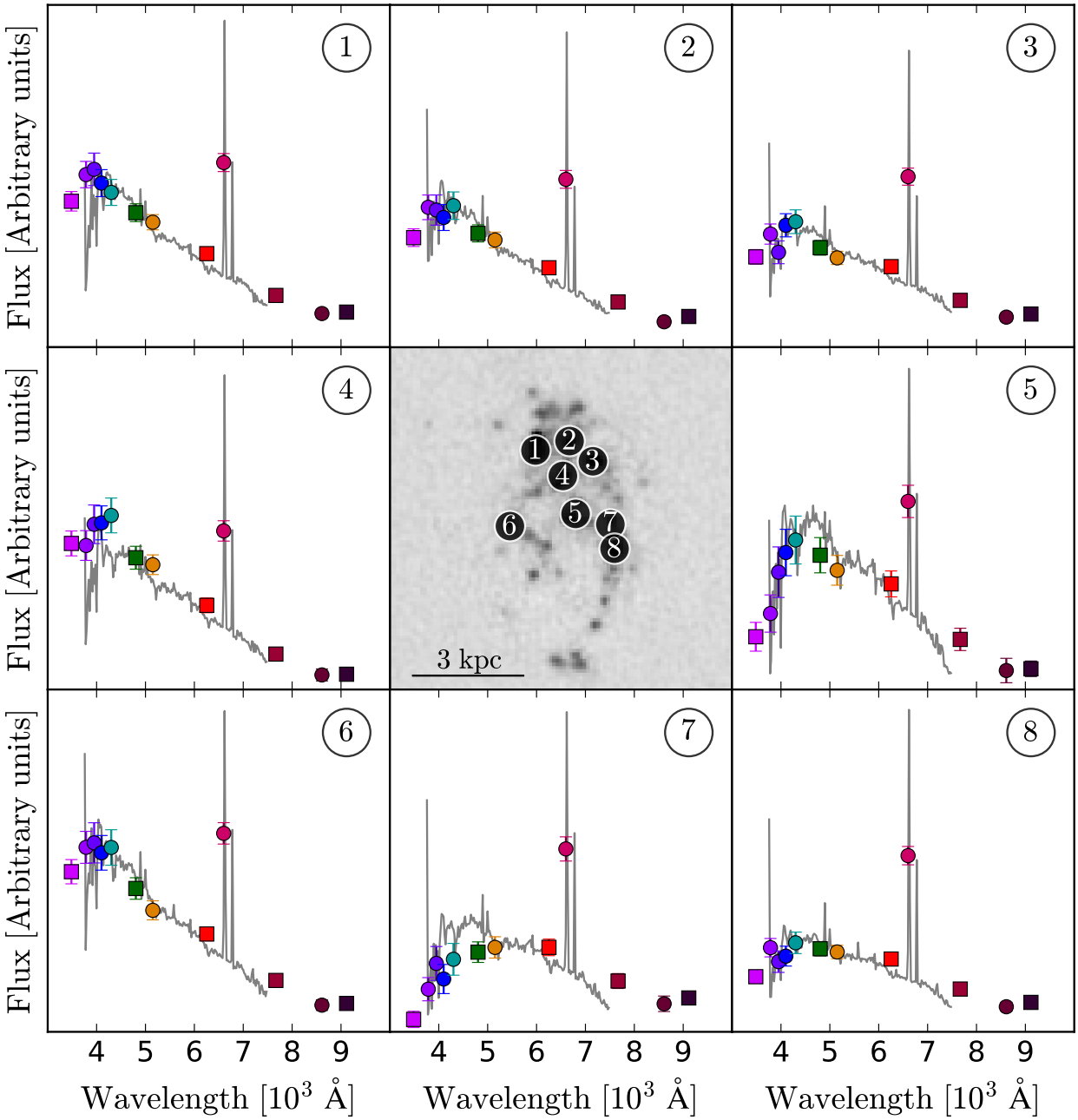

Fig. 6. Eight selected star-forming regions in NGC 4470. *Central panel*: J-PLUS image showing Hα emission areas with the excess in the J0660 band ($J0660-r$), and the selected regions marked with numbers. *Surrounding panels*: J-PLUS SEDs of the corresponding regions, with the CALIFA spectra plotted in gray. The colour code for the bands is the same than in Figs. 1 and 3.

and

$$\sigma_C = \sqrt{\frac{C - C_B}{G}} \tag{7}$$

are the uncertainties associated to the large scale background noise variation and the electron counting, respectively, G is the gain of the detector, N_{pix} is the size of the aperture in pixels, and S_{fit}, a_{fit}, b_{fit} are the resulting coefficients from the background noise empirical model used to calculate this uncertainty (see Labbé et al. 2003; Molino et al. 2014, for details).

The fluxes and errors of every source in every band were calculated following the previous expressions, however, two effects need to be taken into account before getting the final photometric catalogue of the star-forming regions fluxes: (1) the astrometry in the different datasets may have offsets that could introduce mismatches between the location of the regions; (2) the calibration processes differ from one survey to another, bringing up the requirement of having a common scale among them.

In order to minimize aperture displacement effects, the offsets were inspected and corrected in the regions where it was required. To deal with calibration issues, synthetic photometry of the regions was created by convolving their full SDSS/CALIFA spectra with the J-PLUS filters transmission curves, then we matched the synthetic r-band fluxes with the measurements from J-PLUS images and scaled accordingly all the bands, producing the final photometric catalogue. The SEDs and spectra of the star-forming regions were plotted to check the agreement between the different datasets, finding an overall agreement that

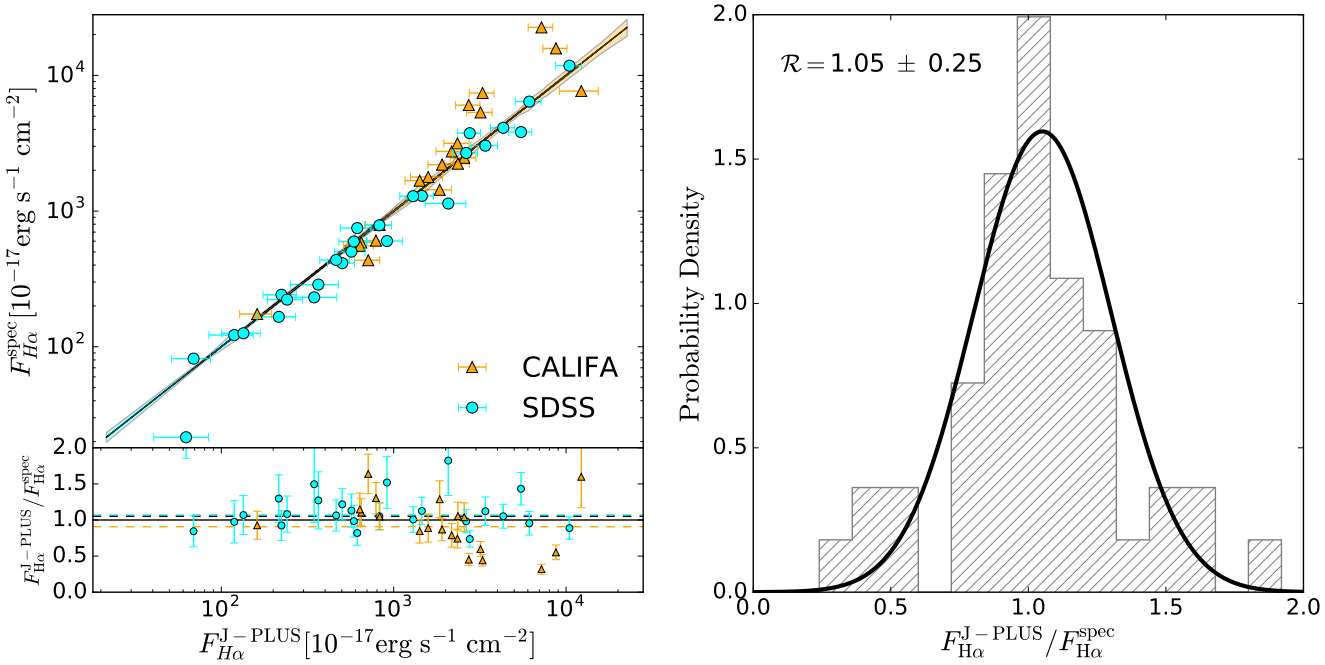

Fig. 7. *Left panel*: comparison between J-PLUS and spectroscopic Hα emission line fluxes. The errorbars represent the J-PLUS uncertainties and the shaded areas the spectroscopic ones. The ratio between the fluxes is shown in the *lower panel*, with the median ratios of CALIFA, SDSS and the total sample represented in orange, blue and black dashed lines, respectively. *Right panel*: normalized distribution of the flux ratios with a Gaussian curve fitted. The median comparison ratio $\mathcal{R}$ and its dispersion are displayed in the panel.

confirms the matching of the regions in terms of astrometry and calibration. As an example, NGC 4470 selected star-forming regions from CALIFA data are presented in Fig. 6. The following step consists of retrieving the dust corrected Hα emission line flux of every star-forming region by using the methodology designed by Vilella-Rojo et al. (2015).

In a previous work, Vilella-Rojo et al. (2015) show that reliable Hα fluxes of star-forming regions in galaxies at $z \leq 0.015$ can be retrieved using the J-PLUS photometric data. In that redshift range, the Hα+[NII] emission is covered by the *J*0660 narrow-band filter, and different methodologies were tested to measure the Hα emission from it. Synthetic J-PLUS data from a sample of 7511 SDSS spectra with measured Hα fluxes were used for this task. The best results were achieved with a three-step process that firstly, starting from the SED of a source, removes the underlying stellar continuum and extracts the Hα+[NII] emission, using a SED-fitting method based on simple stellar population template models from Bruzual & Charlot (2003). Then, the emission from dust extinction in the host galaxy is corrected, making use of a derived empirical relation based on the (*g*–*i*) colour, obtained with SDSS data (Eq. (20) in Vilella-Rojo et al. 2015). Lastly, the [NII] contribution and isolates the Hα emission line flux is removed with another derived empirical relation based also on the (*g*–*i*) colour (Eq. (21) in Vilella-Rojo et al. 2015).

The comparison between the synthetic photometry Hα fluxes and the spectroscopic ones proves that it is possible to get unbiased Hα emission line fluxes with J-PLUS in a robust and homogeneous way. The details of the process can be found in Vilella-Rojo et al. (2015).

The dust corrected Hα emission line fluxes of the J-PLUS photometric data used in the present work were measured with this methodology, using the photometric catalogue (Sect. 3.3) with the SED of every star-forming region. The results are reported in Table 3.

4. Results

In the current section, the collected Hα emission line fluxes of 46 star-forming regions from both spectroscopic CALIFA and SDSS data and photometric J-PLUS data were compared. This was done by computing the comparison ratio $\mathcal{R}$, defined as

$$\mathcal{R} = F_{\mathrm{H}\alpha}^{\mathrm{J-PLUS}} / F_{\mathrm{H}\alpha}^{\mathrm{spec}}, \tag{8}$$

where $F_{\mathrm{H}\alpha}^{\mathrm{J-PLUS}}$ represents the J-PLUS photometric fluxes, and $F_{\mathrm{H}\alpha}^{\mathrm{spec}}$ represents the spectroscopic ones. The median comparison ratio of the 46 star-forming regions analysed here yields $\mathcal{R} = 1.05$, with a 1σ dispersion of 0.25. The results are summarized in Fig. 7.

The comparison between the J-PLUS and the spectroscopic measurements is consistent, being the median $\mathcal{R}$ close to the unit, with a small overestimation of 5%. This deviation is not significant if we consider the low number of regions in the study, and the fact that it lies far below the 1σ uncertainty given by the dispersion. This result is close to the expectations by Vilella-Rojo et al. (2015), that find a median comparison ratio of $\mathcal{R} = 0.99 \pm 0.15$ computed with synthetic J-PLUS photometry. This demonstrates that unbiased Hα emission line fluxes can be measured using J-PLUS photometry.

However, we find that only 63% and 82% of the measurements match each other within an interval of 1σ and 2σ, respectively, pointing out to an underestimation of the uncertainties in the $F_{\mathrm{H}\alpha}^{\mathrm{J-PLUS}}$ values. In order to look deeper into this subject, we computed the variable Δ_F, defined as

$$\Delta_F = \frac{F_{\mathrm{H}\alpha}^{\mathrm{J-PLUS}} - F_{\mathrm{H}\alpha}^{\mathrm{spec}}}{\sigma_{F_{\mathrm{H}\alpha}^{\mathrm{J-PLUS}}}}, \tag{9}$$

where $\sigma_{F_{\mathrm{H}\alpha}^{\mathrm{J-PLUS}}}$ represents the uncertainties associated to the $F_{\mathrm{H}\alpha}^{\mathrm{J-PLUS}}$ values. If these uncertainties are good descriptors of

the accuracy of the measurements, the values of Δ_F should lie in a normal distribution centred around zero with a unit dispersion (e.g. Ilbert et al. 2009; Carrasco Kind & Brunner 2013; López-Sanjuan et al. 2014). In this case, the Δ_F values of the measurements lie normally centred around zero, but the dispersion is 1.29, confirming the underestimation of the uncertainties.

We also observe that the dispersion found in the present work is larger than the one in Vilella-Rojo et al. (2015), 0.25 vs 0.15, respectively. When looking at the individual comparison of the photometric data with each spectroscopic dataset in Fig. 7, offsets in opposite directions are noticeable. One could think that the increase in the dispersion could be caused by the combination of these individual comparisons. However, the median comparison ratio of each spectroscopic dataset is $\mathcal{R} = 1.07 \pm 0.25$ for SDSS and $\mathcal{R} = 0.90 \pm 0.36$ for CALIFA; being the dispersion similar in both cases. It must be considered that in this study, not only are spectroscopic vs. photometric observations being compared, but also all the procedures and codes applied from observations to the final Hα emission line fluxes, such as reduction and calibration processes, continuum fitting with differents SSPs, or emission line modelling among others. All these steps can cause the observed increase in the dispersion with respect to the value given by Vilella-Rojo et al. (2015), done with synthetic J-PLUS photometry.

For this reason, the systematic uncertainty of 15% in the measurements derived by Vilella-Rojo et al. (2015) remains insufficient and needs to be updated to account for the observed uncertainties when the comparison is performed with real data. In fact, by setting a systematic uncertainty of 20%, the Δ_F distribution has a unity dispersion, and 67% and 90% of the measurements match each other within an interval of 1σ and 2σ respectively. This new derived error budget is representative of the uncertainties in the measurements. The results show that the methodology presented in Vilella-Rojo et al. (2015) allows the exploitation of the J-PLUS photometric data in star formation studies in the nearby universe, by providing reliable Hα emission line fluxes and uncertainties.

5. Spatially resolved SFR of NGC 3995 and NGC 3994

It has been reported that galaxies in close interacting pairs can show an enhancement of the SFR in their central parts up to a factor of ten (Patton et al. 2011; Scudder et al. 2012), being higher as the separation of the pair decreases. This enhancement is interpreted as an effect of the turbulence of the infalling gas. The previous studies could not measure Hα emission beyond the centres of the galaxies, since they were carried out with spectroscopic single fibres. Cortijo-Ferrero et al. (2017) observe an enhancement of the SFR in the central parts and the disk of early-stage mergers with CALIFA data. In the J-PLUS SVD 1500041 fields observed for this work, there is a sample of nearby star-forming galaxies, that includes a close pair of interacting galaxies in the initial phase of the merging process: NGC 3995 and NGC 3994 in the triplet Arp313. They are at a projected distance of $r_p = 17.1\,h^{-1}$ kpc (Barton Gillespie et al. 2003). This enables us to study the 2D star formation properties of this pair as an example of the J-PLUS potential in the next section.

5.1. Methods

The objective of this analysis is to get SFR radial profiles and 2D SFR maps of each galaxy. In order to do so, we started with the PSF homogenized images of the field, and then used `SExtractor` (Bertin & Arnouts 1996) to retrieve structural information of the galaxies. The *r*-band image was used with a configuration that allows the code to recognize large galaxies as a single source for this task. The `SExtractor` main configuration parameters to achieve this goal are the DEBLEND_NTHRESH and both the DETECT_MAXAREA and DETECT_MINAREA, that we tuned to get large source detections. In this way, the position, ellipticity, angle of the semi-major axis with respect to the north and half light radius of the galaxies were measured. Next, aperture photometry was performed with `funcnts` on 30 elliptical apertures of increasing radius over the galaxies, from the centre to three half light radii. By making the aperture photometry in terms of the half light radius ($R/R_{\rm eff}$), a common physical scale that allows the comparison of galaxies of different sizes is established. The flux and the error in each aperture were calculated as previously explained in Sect. 3.3. The SED-fitting method and the empirical relations (Sect. 3.3) were applied to the resulting SEDs to get the Hα flux of every elliptical aperture. The SFR of every aperture was estimated with the calibration given by Kennicutt (1998) for a Salpeter (1955) initial mass function (IMF),

$$\mathrm{SFR} = 7.09 \times 10^{-42} L_{\mathrm{H}\alpha} \quad [M_\odot\,\mathrm{yr}^{-1}], \tag{10}$$

where $L_{\mathrm{H}\alpha}$ represents the Hα luminosity,

$$L_{\mathrm{H}\alpha} = 4\pi d_L^2 F_{\mathrm{H}\alpha}, \tag{11}$$

being d_L the luminosity distance estimated with the spectroscopic redshifts of the galaxies (Woods et al. 2006) and $F_{\mathrm{H}\alpha}$ the Hα flux inside a given aperture. Finally, the SFR surface density (Σ_{SFR}) was estimated dividing the SFR by the area of each elliptical aperture. The results are discussed in the following subsections and presented in Fig. 8.

5.2. Results

5.2.1. Total star formation rate

The galaxy NGC 3995 is too big to fit in the FoV of IFUs of surveys such as CALIFA or MaNGA, but not to big for J-PLUS. We measure an SFR of 4.2 ± 0.9 for this galaxy. The estimate by the MPA-JHU group (Brinchmann et al. 2004), is 4.8 ± 4.2, made with a combination of spectroscopic and photometric data from SDSS that induces large uncertainties.

The Sbc spiral NGC 3994 (Sánchez et al. 2012a) has a smaller size, and is part of the sample analysed by CALIFA. We calculated its total SFR to be 2.9 ± 0.6. There are several estimates of the total SFR of this galaxy based on the same CALIFA data: Catalán-Torrecilla et al. (2015) give 5.6 ± 1.4, Sánchez et al. (2016b) measure 3.7 ± 0.4, Cano-Díaz et al. (2016) report 4.5 ± 1.5, and Catalán-Torrecilla et al. (2017) recently estimate 3.16 ± 0.12. The value given by the MPA-JHU group is 1.6 ± 1.3.

The J-PLUS SFR estimates for NGC 3994 and NGC 3995 are compatible with the ones in the literature within 1σ, supporting both the developed methodologies and the quality of the J-PLUS dataset. All the SFR values given have been scaled to a common Salpeter (1955) IMF.

5.2.2. Star formation rate surface density

With all this gathered information, we proceeded to study the Σ_{SFR} of NGC 3995 and NGC 3994 (Fig. 8). In the case of

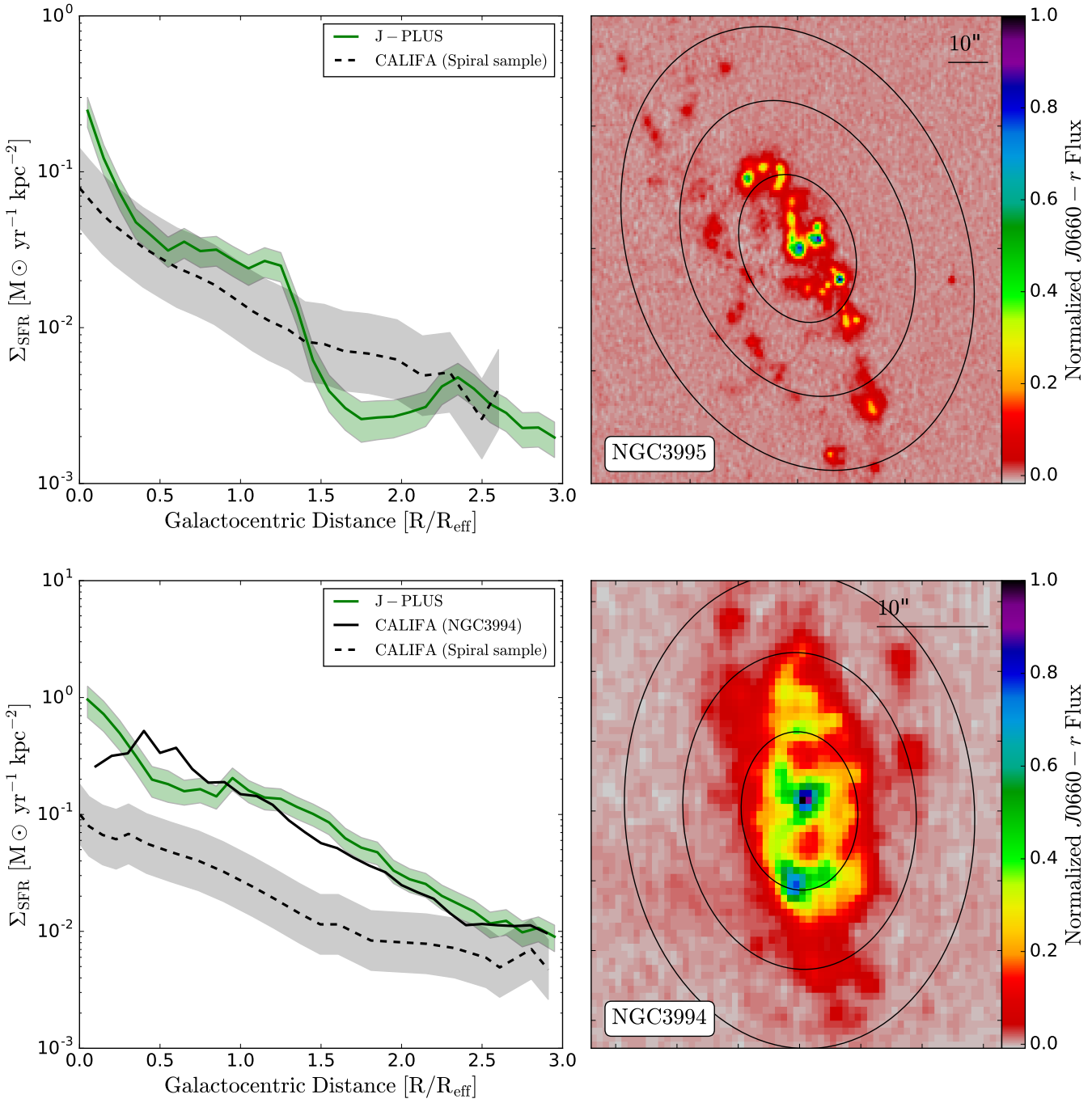

Fig. 8. Star formation rate surface density (Σ_{SFR}) with the shaded area representing the 1σ uncertainty of NGC 3995 (*top left panel*) and NGC 3994 (*bottom left panel*). 2D maps of the excess in the *J*0660 filter (*right panels*), representing the Hα emission areas are shown. One, two, and three R/R_{eff} ellipses are overplotted. The Σ_{SFR} values are compared in each case with a control sample of spirals matched in stellar mass and morphology (dashed black lines). Gray shaded areas show the dispersion of the Σ_{SFR} in the spiral samples. The solid black line (*bottom left panel*) shows the CALIFA Σ_{SFR} measurements of the galaxy. Both the spiral samples and the individual galaxy measurements were performed by González Delgado et al. (2016).

NGC 3995 (upper panel in Fig. 8), the Σ_{SFR} decreases as the galactocentric distance increases. In order to quantify the impact of the interaction in the star formation of NGC 3995, we compared our Σ_{SFR} measurements with the ones of a control sample of non-interacting galaxies matched in morphology and stellar mass from González Delgado et al. (2016). The stellar mass of NGC 3995 was calculated using the empirical relationship given by Taylor et al. (2011) based on the (*g*–*i*) colour of the galaxy, giving a value of log M$_\star$ [$M_\odot$] = 9.52. We find that a Σ_{SFR} enhancement is present not only in the central part of the galaxy but also around 1 R/R_{eff}, in addition, a decrement is observed between 1.4 and 2.4 R/R_{eff}. However, the enhancement is not conclusive, since it is compatible within 2σ with the dispersion in the Σ_{SFR} of the control sample by González Delgado et al. (2016). The abrupt fall observed is most likely related to the distorsion induced by NGC 3994 on the galaxy, which is more evident at the same R/R_{eff} in the Hα excess image, with an assymetry in the distribution of the knots of star formation.

In the case of NGC 3994 (bottom panel in Fig. 8), we also observe how the Σ_{SFR} decreases as the galactocentric distance increases. The derived values for this galaxy are consistent with those found by González Delgado et al. (2016) using CALIFA data with a different methodology, that consists in estimating the fraction of stellar population younger than ∼30 Myr from the spatially-resolved Star Formation History (SFH) of the galaxy, derived by the full spectral synthesis of the data cube (see González Delgado et al. 2016 for details). As in the previous case, we compared our Σ_{SFR} values with the ones of a control sample of non-interacting galaxies matched in morphology and stellar mass from González Delgado et al. (2016). The stellar mass of NGC 3994 was calculated, giving a value of $\log M_\star\ [M_\odot] = 10.41$. In this case, we find a Σ_{SFR} enhancement in the entire disk of the galaxy and not only in the central part. This topic will be tackled in future publications. This is an illustrative example of the science that can be adressed with J-PLUS, carrying out simultaneously spatially resolved and environmental studies in galaxies of all morphological types and sizes in the nearby universe.

6. Summary and conclusions

We have tested the capabilities of measuring Hα emission line fluxes from J-PLUS photometric data by comparing J-PLUS and spectroscopic measurements from SDSS and CALIFA in 46 star-forming regions. We have described the selection and how to retrieve the Hα emission line fluxes from the different datasets. We applied the SED-fitting technique and the empirical relations developed in Vilella-Rojo et al. (2015) to extract the [NII] free and dust corrected Hα fluxes from J-PLUS photometric data. We have performed a comparison between the photometric and spectroscopic Hα emission line fluxes, yielding a median comparison ratio with a scatter of $\mathcal{R} = 1.05 \pm 0.25$, confirming the expectations from Vilella-Rojo et al. (2015) with J-PLUS simulated data.

This result validates the developed methodology to retrieve the Hα flux from J-PLUS data. It provides an unbiased estimator of Hα emission line fluxes, with an error budget representative of the statistical and systematic uncertainties in the measurements. The degree of agreement between the compared fluxes is remarkable, given that we are dealing with photometric and spectroscopic measurements along with their different codes and procedures. The developed methodologies can be also applied to upcoming narrow-band photometric surveys such as S-PLUS and J-PAS.

Finally, we have studied the properties of the 2D star formation in a close pair of interacting galaxies, NGC 3994 and NGC 3995; finding an enhancement of the SFR in the centre and outer parts of the disk of NGC 3994, and obtaining total SFR estimates compatible with values in the literature. It is important to mention that J-PLUS, as a photometric survey, suffers from a lack of spectral resolution. In particular, the restricted number of narrow-band filters limits the number of emission lines that can be measured. This is important for detecting zones in which AGN activity is the main ionizacion source via diagnosis diagrams, and can affect the Hα flux estimates in those areas. These and other issues imposed by the spectral resolution will be further explored in future publications.

Once J-PLUS has completed its planned footprint, we expect to have data for approximately 5000 galaxies at $z \leq 0.015$; a highly suitable dataset to study several science cases related to the star formation in the nearby universe. This represents a significant increase with respect to IFS surveys such as MaNGA, CALIFA, SAMI, or VENGA with 524, 251, 127, and 30 galaxies at the same redshift range respectively.

Acknowledgements. This work is based on observations made with the JAST/T80 telescope at the Observatorio Astrofísico de Javalambre (OAJ), in Teruel, owned, managed and operated by the Centro de Estudios de Física del Cosmos de Aragón. We acknowledge the OAJ Data Processing and Archiving Unit (UPAD) for reducing and calibrating the OAJ data used in this work. Funding for the J-PLUS Project has been provided by the Governments of Spain and Aragón through the Fondo de Inversiones de Teruel, the Aragón Government through the Reseach Groups E96 and E103, the Spanish Ministry of Economy and Competitiveness (MINECO; under grants AYA2015-66211-C2-1-P, AYA2015-66211-C2-2, AYA2012-30789 and ICTS-2009-14), and European FEDER funding (FCDD10-4E-867, FCDD13-4E-2685). R.L.G acknowledges support from "Obra social de la fundación bancaria Ibercaja". K.V. acknowledges the *Juan de la Cierva Incorporación* fellowship, IJCI-2014-21960, of the Spanish government. R.A.D acknowledges support from CNPq through BP grant 312307/2015-2, CSIC through grant COOPB20263, FINEP grants REF. 1217/13-01.13.0279.00 and REF 0859/10-01.10.0663.00 for partial hardware support for the J-PLUS project through the National Observatory of Brazil. L.G. was supported in part by the US National Science Foundation under Grant AST-1311862. R.M.G.D was supported by AYA2016-77846-P, AYA2014-57490-P, and Junta de Andalucía FQ1580. J.A.H.J. and S.A. thank the Brazilian institution CNPq for financial support through post-doctoral fellowship (project 150237/2017-0 and 300336/2016-0, respectively). R.L.O. was partially supported by the Brazilian agency CNPq (Universal Grants 459553/2014-3, PQ 302037/2015-2, and PDE 200289/2017-9). R.L.G wants to thank his thesis directors and CEFCA staff for all the teaching, support and feedback received during the development of this work; to the J-PLUS Collaboration for the feedback received; to the SELGIFS Collaboration (`http://astro.ft.uam.es/selgifs/`) for the training in IFS data management, and to R.M. González Delgado for the data provided for the comparison in Fig. 8. The authors thank the referee for the thorough review. This research made use of `AstroPy` (Astropy Collaboration et al. 2013), `Matplotlib` (Hunter 2007) and `NumPy`, part of the `Python` Software Foundation. (Python Language Reference, version 2.7. Available at `http://www.python.org`). This study uses data provided by the Calar Alto Legacy Integral Field Area (CALIFA) survey (`http://califa.caha.es/`). Based on observations collected at the Centro Astronómico Hispano Alemán (CAHA) at Calar Alto, operated jointly by the Max-Planck-Institut für Astronomie and the Instituto de Astrofísica de Andalucía (CSIC). This study uses data provided by SDSS. Funding for SDSS-III has been provided by the Alfred P. Sloan Foundation, the Participating Institutions, the National Science Foundation, and the US Department of Energy Office of Science. The SDSS-III web site is `http://www.sdss3.org/`. SDSS-III is managed by the Astrophysical Research Consortium for the Participating Institutions of the SDSS-III Collaboration including the University of Arizona, the Brazilian Participation Group, Brookhaven National Laboratory, Carnegie Mellon University, University of Florida, the French Participation Group, the German Participation Group, Harvard University, the Instituto de Astrofisica de Canarias, the Michigan State/Notre Dame/JINA Participation Group, Johns Hopkins University, Lawrence Berkeley National Laboratory, Max Planck Institute for Astrophysics, Max Planck Institute for Extraterrestrial Physics, New Mexico State University, New York University, Ohio State University, Pennsylvania State University, University of Portsmouth, Princeton University, the Spanish Participation Group, University of Tokyo, University of Utah, Vanderbilt University, University of Virginia, University of Washington, and Yale University. This research has made use of the NASA/IPAC Extragalactic Database (NED) which is operated by the Jet Propulsion Laboratory, California Institute of Technology, under contract with the National Aeronautics and Space Administration. This research has made use of the SIMBAD database, operated at CDS, Strasbourg, France (Wenger et al. 2000).

References

Alam, S., Albareti, F. D., Allende Prieto, C., et al. 2015, ApJS, 219, 12
Astropy Collaboration (Robitaille, T. P., et al.) 2013 A&A, 558, A33
Bacon, R., Copin, Y., Monnet, G., et al. 2001, MNRAS, 326, 23
Bacon, R., Accardo, M., Adjali, L., et al. 2010, Proc. SPIE, 7735, 773508
Baldwin, J. A., Phillips, M. M., & Terlevich, R. 1981, PASP, 93, 5
Barrera-Ballesteros, J. K., Sánchez, S. F., García-Lorenzo, B., et al. 2015, A&A, 579, A45
Barton Gillespie, E., Geller, M. J., & Kenyon, S. J. 2003, ApJ, 582, 668
Benitez, N., Dupke, R., Moles, M., et al. 2014, ArXiv e-prints [arXiv: 1403.5237]
Bertin, E. 2011, in Astronomical Data Analysis Software and Systems XX, eds. I. N. Evans, A. Accomazzi, D. J. Mink, & A. H. Rots, ASP Conf. Ser., 442, 435

Bertin, E. 2013, Astrophysics Source Code Library [record ascl:1301.001]
Bertin, E., & Arnouts, S. 1996, A&AS, 117, 393
Blanc, G. A., Weinzirl, T., Song, M., et al. 2013, AJ, 145, 138
Bonatto, C., Chies-Santos, A. L., Coelho, P. R. T., et al. (J-PLUS Collaboration) 2019, A&A, 622, A179
Brinchmann, J., Charlot, S., White, S. D. M., et al. 2004, MNRAS, 351, 1151
Bruzual, G., & Charlot, S. 2003, MNRAS, 344, 1000
Bundy, K., Bershady, M. A., Law, D. R., et al. 2015, ApJ, 798, 7
Calzetti, D. 2013, in Star Formation Rate Indicators, eds. J. Falcón-Barroso, & J. H. Knapen, 419
Calzetti, D., Armus, L., Bohlin, R. C., et al. 2000, ApJ, 533, 682
Cano-Díaz, M., Sánchez, S. F., Zibetti, S., et al. 2016, ApJ, 821, L26
Cappellari, M., Emsellem, E., Krajnović, D., et al. 2011, MNRAS, 413, 813
Carrasco Kind, M., & Brunner, R. J. 2013, MNRAS, 432, 1483
Catalán-Torrecilla, C., Gil de Paz, A., Castillo-Morales, A., et al. 2015, A&A, 584, A87
Catalán-Torrecilla, C., Gil de Paz, A., Castillo-Morales, A., et al. 2017, ApJ, 848, 87
Cenarro, A. J., Cristóbal-Hornillos, D., Marín-Franch, A., et al. (J-PLUS Collaboration) 2019, A&A, 622, A176
Cortijo-Ferrero, C., González Delgado, R. M., Pérez, E., et al. 2017, A&A, 607, A70
Croom, S. M., Lawrence, J. S., Bland-Hawthorn, J., et al. 2012, MNRAS, 421, 872
Drory, N., MacDonald, N., Bershady, M. A., et al. 2015, AJ, 149, 77
Falcón-Barroso, J., Sánchez-Blázquez, P., Vazdekis, A., et al. 2011, A&A, 532, A95
Gallego, J., Zamorano, J., Aragon-Salamanca, A., & Rego, M. 1996, ApJ, 459, L43
García-Benito, R., Zibetti, S., Sánchez, S. F., et al. 2015, A&A, 576, A135
Gil de Paz, A., Carrasco, E., Gallego, J., et al. 2016, Proc. SPIE, 9908 99081K
González Delgado, R. M., Cid Fernandes, R., Pérez, E., et al. 2016, A&A, 590, A44
Hunter, J. D. 2007, Comput. Sci. Eng., 9, 90
Ilbert, O., Capak, P., Salvato, M., et al. 2009, ApJ, 690, 1236
Kauffmann, G., Heckman, T. M., Tremonti, C., et al. 2003, MNRAS, 346, 1055
Kennicutt, Jr. R. C. 1998, ARA&A, 36, 189
Kennicutt, R. C., & Evans, N. J. 2012, ARA&A, 50, 531
Kewley, L. J., Dopita, M. A., Sutherland, R. S., Heisler, C. A., & Trevena, J. 2001, ApJ, 556, 121
Koyama, Y., Smail, I., Kurk, J., et al. 2013, MNRAS, 434, 423
Labbé, I., Franx, M., Rudnick, G., et al. 2003, AJ, 125, 1107
López-Sanjuan, C., Cenarro, A. J., Hernández-Monteagudo, C., et al. 2014, A&A, 564, A127
López-Sanjuan, C., Vázquez-Ramió, H., Varela, J., et al. (J-PLUS Collaboration) 2019, A&A, 622, A177
Mandel, E., Murray, S. S., & Roll, J. B. 2001, in Astronomical Data Analysis Software and Systems X, eds. F. R. Harnden, Jr., F. A. Primini, & H. E. Payne, ASP Conf. Ser., 238, 225
Maraston, C., & Strömbäck, G. 2011, MNRAS, 418, 2785
Marin-Franch, A., Taylor, K., Cenarro, J., Cristobal-Hornillos, D., & Moles, M. 2015, IAU General Assembly, 22, 2257381
Molino, A., Benítez, N., Moles, M., et al. 2014, MNRAS, 441, 2891
Molino, A., Costa-Duarte, M. V., Mendes de Oliveira, C., et al. (J-PLUS Collaboration) 2019, A&A, 622, A178
Oke, J. B., & Gunn, J. E. 1983, ApJ, 266, 713
Patton, D. R., Ellison, S. L., Simard, L., McConnachie, A. W., & Mendel, J. T. 2011, MNRAS, 412, 591
Pérez-González, P. G., Gallego, J., Zamorano, J., et al. 2003, ApJ, 587, L27
Roth, M. M., Kelz, A., Fechner, T., et al. 2005, PASP, 117, 620
Salpeter, E. E. 1955, ApJ, 121, 161
Sánchez, S. F., García-Lorenzo, B., Jahnke, K., et al. 2006, New Astron. Rev., 49, 501
Sánchez, S. F., Rosales-Ortega, F. F., Kennicutt, R. C., et al. 2011, MNRAS, 410, 313
Sánchez, S. F., Kennicutt, R. C., Gil de Paz, A., et al. 2012a, A&A, 538, A8
Sánchez, S. F., Rosales-Ortega, F. F., Marino, R. A., et al. 2012b, A&A, 546, A2
Sánchez, S. F., García-Benito, R., Zibetti, S., et al. 2016a, A&A, 594, A36
Sánchez, S. F., Pérez, E., Sánchez-Blázquez, P., et al. 2016b, Rev. Mex. Astron. Astrofis., 52, 171
Sánchez, S. F., Pérez, E., Sánchez-Blázquez, P., et al. 2016c, Rev. Mex. Astron. Astrofis., 52, 21
Sánchez, S. F., Avila-Reese, V., Hernandez-Toledo, H., et al. 2018, Rev. Mex. Astron. Astrofis., 54, 217
Sánchez-Blázquez, P., Peletier, R. F., Jiménez-Vicente, J., et al. 2006, MNRAS, 371, 703
San Roman, I., Sánchez-Blázquez, P., Cenarro, A. J., et al. (J-PLUS Collaboration) 2019, A&A, 622, A181
Santini, P., Rosario, D. J., Shao, L., et al. 2012, A&A, 540, A109
Sarzi, M., Falcón-Barroso, J., Davies, R. L., et al. 2006, MNRAS, 366, 1151
Schaefer, A. L., Croom, S. M., Allen, J. T., et al. 2017, MNRAS, 464, 121
Scudder, J. M., Ellison, S. L., Torrey, P., Patton, D. R., & Mendel, J. T. 2012, MNRAS, 426, 549
Speagle, J. S., Steinhardt, C. L., Capak, P. L., & Silverman, J. D. 2014, ApJS, 214, 15
Stefanon, M., Yan, H., Mobasher, B., et al. 2017, ApJS, 229, 32
Strauss, M. A., Weinberg, D. H., Lupton, R. H., et al. 2002, AJ, 124, 1810
Taylor, E. N., Hopkins, A. M., Baldry, I. K., et al. 2011, MNRAS, 418, 1587
Thomas, D., Steele, O., Maraston, C., et al. 2013, MNRAS, 431, 1383
Vazdekis, A., Sánchez-Blázquez, P., Falcón-Barroso, J., et al. 2010, MNRAS, 404, 1639
Vilella-Rojo, G., Viironen, K., López-Sanjuan, C., et al. 2015, A&A, 580, A47
Wake, D. A., Bundy, K., Diamond-Stanic, A. M., et al. 2017, AJ, 154, 86
Walcher, C. J., Wisotzki, L., Bekeraité, S., et al. 2014, A&A, 569, A1
Wenger, M., Ochsenbein, F., Egret, D., et al. 2000, A&AS, 143, 9
Willett, K. W., Schawinski, K., Simmons, B. D., et al. 2015, MNRAS, 449, 820
Woods, D. F., Geller, M. J., & Barton, E. J. 2006, AJ, 132, 197
York, D. G., Adelman, J., Anderson, Jr., J. E., et al. 2000, AJ, 120, 1579

[1] Centro de Estudios de Física del Cosmos de Aragón (CEFCA), Plaza San Juan 1, 44001 Teruel, Spain
e-mail: rlgarcia@cefca.es
[2] Centro de Estudios de Física del Cosmos de Aragón (CEFCA), Unidad Asociada al CSIC, Plaza San Juan 1, 44001 Teruel, Spain
[3] Observatório Nacional/MCTIC, Rua Gen. José Cristino, 77, 20921-400 Rio de Janeiro, Brazil
[4] Departamento de Astronomia, Instituto de Física, Universidade Federal do Rio Grande do Sul, Porto Alegre, Brazil
[5] Universidade de Sao Paulo, Instituto de Astronomia, Geofísica e Ciências Atmosféricas, Rua do Matao, 1226, Sao Paulo 05508-900, Brazil
[6] Department of Astronomy, University of Michigan, Ann Arbor, MI 48109-1107, USA
[7] PITT PACC, Department of Physics and Astronomy, University of Pittsburgh, Pittsburgh, PA 15260, USA
[8] IAA (CSIC), Glorieta de la Astronomía s/n, 18008 Granada, Spain
[9] Universidade Federal de Sergipe, Departamento de Física, Av. Marechal Rondon, s/n, 49000-000 Sao Cristóvao, SE, Brazil
[10] X-ray Astrophysics Laboratory, NASA Goddard Space Flight Center, Greenbelt, MD 20771, USA
[11] Department of Physics, University of Maryland, Baltimore County, 1000 Hilltop Circle, Baltimore, MD 21250, USA
[12] Institute for Astronomy, University of Edinburgh, Royal Observatory, Blackford Hill, Edinburgh EH9 3HJ, UK
[13] European Southern Observatory, Karl-Schwarzschild-Str. 2, 85748 Garching, Germany
[14] Observatório do Valongo, Universidade Federal do Rio de Janeiro, Ladeira Pedro Antonio 43, 20080-090 Rio de Janeiro, Brazil
[15] European Space Astronomy Centre (ESAC)/ESA, PO Box 78, 28690 Villanueva de la Canada Madrid, Spain